HUMAN GENE THERAPY 23:210–217 (February 2012)

DOI: 10.1089/hum.2011.162

Safety and Tolerability of Magnetic Resonance Imaging-Guided Convection-Enhanced Delivery of AAV2-hAADC with a Novel Delivery Platform in Nonhuman Primate Striatum

Waldy San Sebastian,[1,*] R. Mark Richardson,[1,*] Adrian P. Kells,[1] Clementine Lamarre,[1] John Bringas,[1] Philip Pivirotto,[1] Ernesto A. Salegio,[1] Stephen J. DeArmond,[2] John Forsayeth,[1] and Krystof S. Bankiewicz[1]

Abstract

Degeneration of nigrostriatal neurons in Parkinson's disease (PD) causes progressive loss of aromatic L-amino acid decarboxylase (AADC), the enzyme that converts levodopa (L-DOPA) into dopamine in the striatum. Because loss of this enzyme appears to be a major driver of progressive impairment of response to the mainstay drug, L-DOPA, one promising approach has been to use gene therapy to restore AADC activity in the human putamen and thereby restore normal L-DOPA response in patients with PD. An open-label phase I clinical trial of this approach in patients with PD provided encouraging signs of improvement in Unified Parkinson's Disease Rating Scale scores and reductions in antiparkinsonian medications. However, such improvement was modest compared with the results previously reported in parkinsonian rhesus macaques. The reason for this discrepancy may have been that the relatively small volume of vector infused in the clinical study restricted the distribution of AADC expression, such that only about 20% of the postcommissural putamen was covered, as revealed by L-[3-^{18}F]-α-methyltyrosine-positron emission tomography. To achieve more quantitative distribution of vector, we have developed a visual guidance system for parenchymal infusion of AAV2. The purpose of the present study was to evaluate the combined magnetic resonance imaging-guided delivery system with AAV2-hAADC under conditions that approximate the intended clinical protocol. Our data indicate that this approach directed accurate cannula placement and effective vector distribution without inducing any untoward effects in nonhuman primates infused with a high dose of AAV2-hAADC.

Introduction

Parkinson's disease (PD) is a neurodegenerative disease characterized in part by the loss of dopaminergic neurons of the substantia nigra pars compacta. Degeneration of nigrostriatal neurons causes progressive loss of aromatic L-amino acid decarboxylase (AADC), the enzyme that converts levodopa (L-DOPA) into dopamine in the striatum. A promising approach has been to attempt the restoration of near-normal levels of AADC by the striatal convection-enhanced delivery (CED) of an adeno-associated virus type 2 (AAV2) vector carrying the human AADC (hAADC) gene. CED is a pressurized parenchymal infusion technique that allows therapeutic agents to be distributed throughout large volumes of brain (Bobo *et al.*, 1994). CED of AAV2-hAADC results in robust, essentially permanent, gene expression in the striatum and its beneficial effect has been demonstrated in several preclinical studies in rodent and nonhuman primate (NHP) models of PD (Bankiewicz *et al.*, 2000, 2006; Sanchez-Pernaute *et al.*, 2001; Forsayeth *et al.*, 2006; Hadaczek *et al.*, 2010). These preclinical studies led to a phase I clinical trial in patients with PD (Eberling *et al.*, 2008; Christine *et al.*, 2009; Valles *et al.*, 2010), in which two cohorts of patients with moderately advanced PD received a bilateral infusion of either a low or high dose of AAV2-hAADC vector into the putamen. Although patients showed apparent improvement in terms of Unified Parkinson's Disease Rating Scale (UPDRS) scores and reductions in antiparkinsonian medications, such improvement was modest compared with the results previously reported in parkinsonian NHP (Bankiewicz *et al.*, 2006). The reason for this discrepancy may have been that the relatively small volume of vector infused in the clinical study

[1]Department of Neurological Surgery, University of California San Francisco, San Francisco, 94103 CA.
[2]Department of Pathology and Department of Laboratory Medicine, University of California San Francisco, San Francisco, 94103 CA.
*These authors contributed equally to this work.

(100 μl per hemisphere) restricted the distribution of AADC expression, revealed by L-[3-^{18}F]-α-methyltyrosine-positron emission tomography (FMT-PET) (Eberling *et al.*, 2008), such that only about 20% of the postcommissural putamen was covered. The stereotactic infusion parameters for the clinical study were identical to those used in the preclinical NHP study and were considered, therefore, to have at least a 5-fold margin of safety based on volumetric differences between human and NHP putamen (Yin *et al.*, 2009). To achieve more quantitative distribution of vector, we have developed a visual guidance system for parenchymal infusion of AAV2 (Fiandaca *et al.*, 2009). In this approach, the magnetic resonance imaging (MRI) tracer, gadoteridol (Gd; Bracco Diagnostics USA, Princeton, NH), is included with the AAV2-hAADC and the infusion is conducted in an MR magnet. Because the acute tracer distribution matches the distribution of transgene expression (Fiandaca *et al.*, 2009), Gd can be used as a real-time surrogate for visualizing vector infusion. We have evolved a method for visually monitored CED (real-time convective delivery, or RCD) that has been modeled extensively in NHP (Fiandaca *et al.*, 2008, 2009; Richardson *et al.*, 2009, 2011a,b; Gimenez *et al.*, 2011). This innovation not only reduces the potential for adverse effects but also provides surgeons with intraoperative feedback on infusate distribution. Studies from our group demonstrate the high precision, predictability, and safety of this RCD system for parenchymal AAV2-GDNF (glial cell line-derived neurotrophic factor) delivery in NHP (Richardson *et al.*, 2011b). In this paper, we report the safety and tolerability of RCD-mediated AAV2-hAADC therapy with a novel, U.S. Food and Drug Administration (FDA)-approved, interventional MRI (iMRI)-based clinical delivery platform in order to model in NHP a planned AAV2-hAADC gene therapy trial in patients with PD. Our data indicate that this approach directed accurate cannula placement and effective vector distribution without inducing any untoward effects in NHP infused with a high dose of AAV2-hAADC. This study supports clinical use of this new gene delivery technology.

Materials and Methods

Animals

Ten adult female rhesus monkeys (*Macaca mulatta*, 5.2–12.8 kg) were lesioned with 1-methyl-4-phenyl-1,2,3,6-tetrahydropyridine (MPTP) as previously described (Bankiewicz *et al.*, 1986, 2000; Eberling *et al.*, 1998). Briefly, MPTP lesioning consisted of one right intracarotid artery infusion of 2.0–4.0 mg of MPTP-HCl. Behavioral assessment was performed that indicated mild to moderate parkinsonism. This model is characterized by almost complete nigrostriatal lesioning of the ipsilateral hemisphere with little or no effect on the contralateral hemisphere (Eberling *et al.*, 1998). Experiments were performed according to National Institutes of Health (Bethesda, MD) guidelines and to protocols approved by the Institutional Animal Care and Use Committee at the University of California San Francisco (San Francisco, CA).

Behavioral assessment

The modified Parkinson Clinical Rating Scale (CRS) employed here was developed in our laboratory and closely approximates those reported in the literature (Imbert *et al.*, 2000). The scale evaluates 14 parkinsonian features, each of which receives a score from 0 to 3 in order of increasing severity. Individual scores are summed to arrive at a final score. Features evaluated include tremor (right and left sides), locomotion, "freezing," fine motor skills (right and left sides), bradykinesia (right and left sides), hypokinesia, balance, posture, startle response, and gross motor skills (right and left sides). Normal animals score in the range 0–4 and severely parkinsonian monkeys score above 21. An experienced rater, blinded to treatment group, performed all measurements.

Vector production

The human AADC cDNA was cloned into an AAV2 shuttle plasmid, and a recombinant AAV2 carrying hAADC under the control of the cytomegalovirus promoter was manufactured by the AAV Clinical Vector Core at Children's Hospital of Philadelphia (Philadelphia, PA) as previously described (Matsushita *et al.*, 1998; Wright *et al.*, 2003). AAV2-hAADC was purified from cell extracts by CsCl centrifugation and was concentrated to approximately 7.2×10^{12} vector genomes (VG)/ml.

Surgical procedure

Two weeks before infusion, NHP underwent stereotactic placement of a skull-mounted, MRI-compatible, threaded plastic adaptor plug (diameter, 12 mm; height, 14 mm) for later attachment of frame. After craniectomy, the plug was secured to the skull over the right hemisphere with dental acrylic. After placement of the adaptor plug, animals recovered for at least 2 weeks before initiation of iMRI infusion procedures. Only animals receiving AAV2-hAADC underwent MRI-guided CED; control animals were infused with phosphate-buffered saline (PBS) via SmartFlow catheter in a stereotactic frame but without image guidance.

ClearPoint system, target selection, trajectory planning, and cannula insertion

Both the delivery system and the procedure have been described previously in detail (Richardson *et al.*, 2011a,b). Briefly, the ClearPoint system (MRI Interventions [formerly SurgiVision], Memphis, TN) consists of the SmartFrame, an infusion cannula (SmartFlow), and a software system that communicates with both the MRI console and the operating neurosurgeon in the MRI suite. The SmartFrame houses an MRI-visible (gadolinium-impregnated) fluid stem and integrated fiducials that are detected by the software. On the day of infusion, NHP were sedated with intramuscular ketamine–xylazine (7 and 3 mg/kg, respectively), intubated, and placed on inhaled isoflurane (1–3%). The plug adaptor was prepared under sterile conditions and the NHP was placed supine in an MRI-compatible stereotactic frame. The SmartFrame was attached by screwing the base onto the adaptor plug over the right hemisphere. The NHP was moved into the bore and a controller was attached to the SmartFrame, which allows the surgeon to manually "dial in" distance changes to align the cannula to the desired trajectory in four directions (pitch, roll, anterior–posterior, medial–lateral) as instructed by the ClearPoint software.

First, a high-resolution anatomical MR scan was acquired for target identification and surgical planning. Images were

then transferred to the ClearPoint system, where the target for cannula tip placement was selected. In all animals, two precommissural locations in the right hemisphere: one in the caudate nucleus and one in the putamen were selected.

Next, rapid scans were obtained that allowed the ClearPoint software to detect the position and orientation of the SmartFrame fluid stem. The software used this image to compare the current SmartFrame trajectory with the target trajectory and generate instructions to adjust SmartFrame alignment via the pitch and roll controls. After these adjustments were made, the image was reacquired to measure the new expected error and this process was repeated as necessary. When the expected error was within 1.0 mm, the pitch and roll axes were locked and more scans were acquired along the sagittal and coronal planes of the guide stem for fine adjustment of the SmartFrame *x–y* stage. This process was repeated until the software reported an expected error of <0.5 mm, typically requiring no more than two iterations.

The infusion system included FDA-approved SmartFlow catheter, a custom-designed, ceramic, fused silica reflux-resistant cannula with a 3-mm stepped tip (Krauze *et al.*, 2005; Fiandaca *et al.*, 2008). The cannula was attached to a 1-ml syringe mounted onto an MRI-compatible infusion pump (Harvard Bioscience, Holliston, MA). Infusion was initiated at 1 μl/min and, after visualizing fluid flow from the cannula tip when held at the height of the head of the NHP, the cannula was inserted through the SmartFrame guide stem and into the brain. When the depth stop encountered the top of the guide stem, it was secured with a locking screw.

Infusion and imaging data analysis

Infusions were performed as previously described in more detail (Richardson *et al.*, 2011a,b). After cannula insertion, repeated multiplanar FLASH (fast low angle shot) images were obtained every 5 min for the duration of the infusion. After visualization of Gd infusion at the cannula tip, the infusion rate was ramped up from an initial 1 μl/min to a maximum of 3 μl/min by 0.5-μl/min increments every 5 min. Each NHP first received an infusion in the right putamen (50 μl) and then in the right caudate nucleus (50 μl). Distribution volumes of Gd were measured with OsiriX, an open source DICOM (Digital Imaging and Communications in Medicine) reader and imaging workstation. Software was written and applied as an OsiriX plug-in to auto-segment each infusion on individual MRI slices from which a total infusion volume was calculated.

Tissue processing

Each NHP was perfused transcardially with PBS and PBS–4% paraformaldehyde–0.1% glutaraldehyde $\sim$8 months after the infusion session and 3–8 weeks after L-DOPA injections. Sectioning and immunostaining of brain tissue were performed as previously described (Richardson *et al.*, 2011b). Briefly, brains were harvested, sliced in 3-mm coronal sections in a brain matrix, postfixed in PBS–4% paraformaldehyde, and cryoprotected in 30% (w/v) sucrose. A sliding microtome was used to cut 40-μm serial sections for histological processing. For immunohistochemistry, sections were first washed in PBS followed by treatment with 3% H_2O_2 in PBS to block endogenous peroxidase. Sections were then incubated in Sniper blocking solution (Biocare Medical, Concord, CA) followed by incubation with the corresponding primary antibody: rabbit polyclonal anti-DOPA decarboxylase (DDC), diluted 1:1000 (AB136; Millipore, Bedford, MA); anti-Iba1 (microglial cell marker), diluted 1:1000 (CP290; Biocare Medical); mouse monoclonal anti-tyrosine hydroxylase (TH), diluted 1:5000 (MAB318; Millipore); mouse monoclonal anti-glial fibrillary acidic protein (GFAP), diluted 1:100,000 (MAB360; Millipore) in Da Vinci green diluent (Biocare Medical) overnight at ambient temperature (for DDC and TH) or 4°C (for Iba1 and GFAP). Sections were rinsed in PBS and incubated in the corresponding MACH 2 horseradish peroxidase (HRP) polymer (Biocare Medical) for 1 hr, followed by several washes and colorimetric development with 3,3′-diaminobenzidine (DAB). GFAP-immunostained sections were also counterstained with cresyl violet. Immunostained sections were mounted on slides and sealed with a toluene-based mounting medium (Shandon-Mount; Thermo Fisher Scientific, Waltham, MA). For hematoxylin and eosin (H&E) staining, free-floating sections were rehydrated and stained with hematoxylin for 3 min, washed with water, and then differentiated in 0.5% glacial acetic acid–70% alcohol followed by staining in bluing solution. After incubation in eosin, the sections were dehydrated in alcohol and xylene, and coverslipped. H&E-stained sections were analyzed in a blinded manner by a board-certified pathologist (S.D.).

Results

Performance of delivery platform and cannula

The SmartFlow cannula and ClearPoint targeting system (with SmartFrame skull attachment modified for NHP use; Richardson *et al.*, 2011a) were used (Fig. 1) to infuse either AAV2-hAADC ($n=6$) or PBS ($n=4$) to the right caudate nucleus and putamen (total of 20 cannula insertions). The two infusions per NHP were performed sequentially during the same procedure with no technical limitations encountered in redirecting the cannula for infusion of the second site. The ratio of volume of distribution (V_d) to volume of infusion (V_i) relationship (V_d/V_i) is important in real-time CED for planning drug doses and was calculated for each infusion. The mean V_d/V_i ratio was 1.6 (95% confidence interval [CI], 0.3) and 3.1 (95% CI, 0.6) for caudate nucleus and putamen, respectively; the latter similar to that previously reported for NHP putamen (Richardson *et al.*, 2011b). No MRI-visible hemorrhages occurred during cannula placement, and no adverse effects occurred during RCD or subsequently. However, some leakage of infusate was observed dorsally into the internal capsule in one of the animals during the putaminal infusion (Fig. 2), although no pathological signs were observed in this animal immediately after surgery or subsequently.

Intervention-related pathology

H&E staining and GFAP or Iba1 immunohistochemistry were performed to assess any tissue damage related to the surgery. H&E staining showed no evidence of overt pathology, such as cerebritis, infarcts or cellular infiltrates around the delivery sites in any of the animals, control or AAV2-hAADC (Fig. 3, left and middle columns). Only a moderate

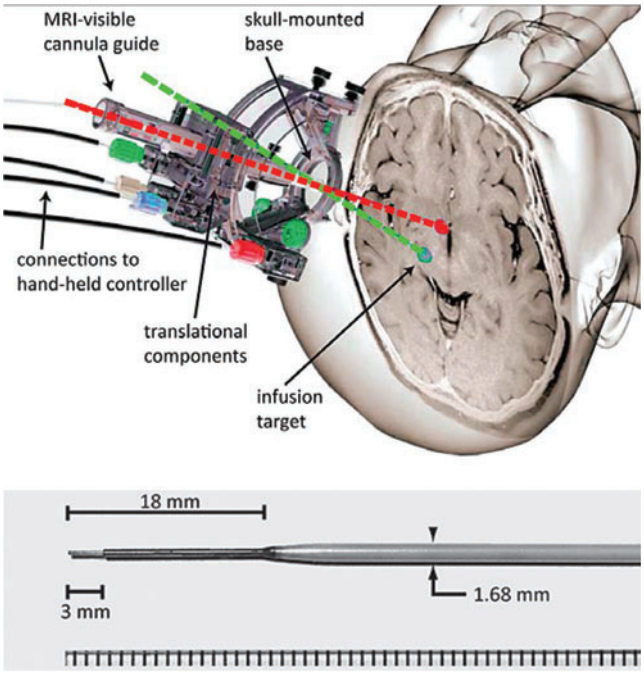

FIG. 1. *Top:* MRI-compatible stereotactic aiming device and cannula. SmartFrame stereotactic aiming device includes a skull-mounted holder for the infusion cannula and controls that permit adjustment of the trajectory while the patient is in the MR bore. Planning and intraoperative adjustment are accomplished with the aim of ClearPoint software as described in more detail by Richardson and colleagues (2011a). *Bottom:* The SmartFlow MRI-compatible cannula. The step in the outer dimensions prevents infusate reflux. Color images available online at www.liebertonline.com/hum

inflammatory reaction to the cannula insertion could be seen. This reaction was confined to the area surrounding the cannula tract, where the presence of standard lymphocytes and macrophages containing some hemosiderin was noticed. The rest of the target region appeared normal. Also, the white matter around the target nuclei (caudate nucleus and putamen) was spared and looked the same in both the ipsilateral and contralateral hemispheres. One animal that received AAV2-hAADC, however, presented with some cellular infiltration that correlated with the spread of infusate in the striatum and internal capsule (Fig. 3, right-hand column). Analysis of H&E-stained sections at high magnification from this animal evinced some reactive astrocytes (gliosis) and many lymphocytes in the corona radiata leakage area, indicative of chronic inflammation. Curiously, some eosinophils were also detected in this region. The presence of this type of blood cell is unusual in the brain parenchyma and suggestive of an infection as the cause of the inflammatory process detected. However, this animal presented no subsequent behavioral signs or other pathology related to the leakage. One of the animals in the control group exhibited pathological signs of hemorrhage close to the infusion area in the putamen that was revealed during gross anatomical inspection of the postmortem brain. However, the animal did not show any pathological behavior or signs.

In each animal, regardless of control or active group assignment, moderate Iba1 and GFAP expression was noted along the cannula tracts and at the depth of the proximal, fused silica tip (Fig. 3b and c), consistent with previous reports demonstrating slight inflammation after CED from a stepped cannula (Su *et al.*, 2009). In all animals, areas of both caudate nucleus and putamen 0.75 mm away from the infusion site were not considered positive by H&E staining, or by GFAP and Iba1 staining, because they exhibited basal expression of these markers.

High-dose AAV2-hAADC vector distribution

The open label phase I clinical trial investigated two dose levels (9.0×10^{10} and 3.0×10^{11} VG) with a higher planned dose (9.0×10^{11} VG) not conducted because of manufacturing constraints. Some patients in this trial displayed a modest improvement in UPDRS score in both off- and on-medication states (Christine *et al.*, 2009). However, retrospective comparison with an earlier dose-ranging study in NHP (1.2×10^{10} to 1.0×10^{12} VG) suggests that the doses in the phase I trial were at the threshold for expected therapeutic effect when adjusted for the 5-fold difference in striatum volume between humans and NHP. Thus, a higher dose and greater infusion volumes should be investigated in future studies.

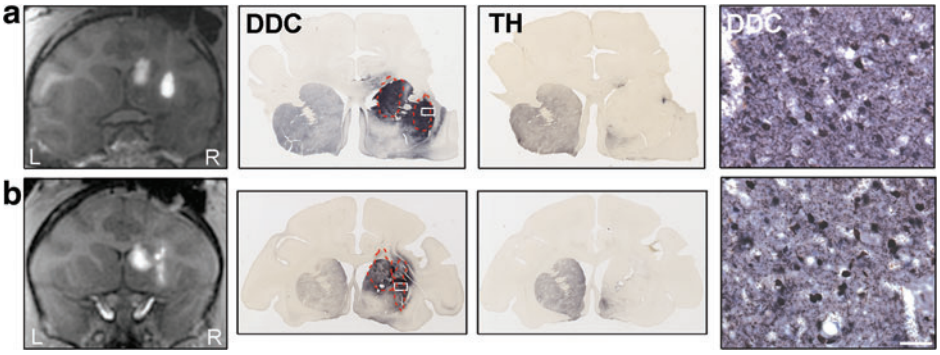

FIG. 2. Correlation between gadoteridol and AADC expression. MRI images (first column) show gadoteridol distribution at the end of both caudate nucleus and putamen CED after **(a)** an uneventful AAV2-hAADC infusion and **(b)** one with significant infusate leakage dorsally into the internal capsule. Images in the second column correspond to immunoperoxidase staining for AADC at the same level as the MRI pictures. Dashed red lines correspond to the gadolinium signal area from the MRI images. Third column images demonstrate the extent of MPTP-induced lesion as shown by TH immunostaining of a brain section adjacent to an anti-AADC-stained section. Pictures in the last column were obtained at higher magnification in the putamen (white boxes in AADC low-magnification images) and show robust striatal expression of the hAADC transgene with a large number of AADC-transduced neurons and fibers. Scale bar: 50 μm. DDC, DOPA decarboxylase. Color images available online at www.liebertonline.com/hum

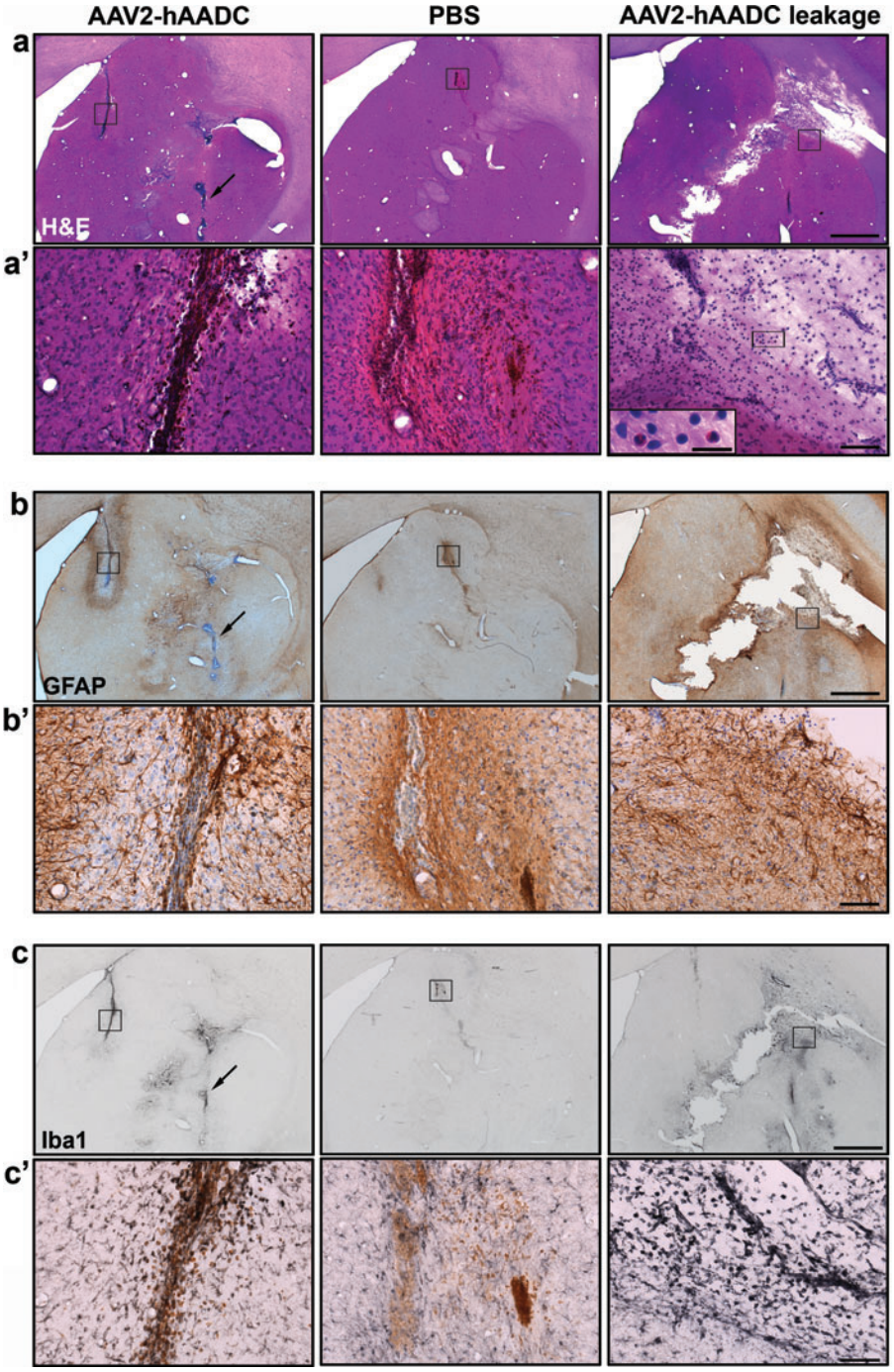

FIG. 3. Lack of tissue damage in target structures. Representative images show cannula tracts with H&E **(a** and **a′)**, GFAP **(b** and **b′),** or Iba1 **(c** and **c′)** immunostaining in AAV2-hAADC-treated NHP (left-hand column), PBS control (middle column) animals, and an AAV2-hAADC-treated animal with infusate leakage dorsally into the internal capsule (right-hand column). H&E staining evinced no tissue damage in either AAV2-hAADC-treated (**a**, left) or in control (**a**, middle) animals. Similarly, in adjacent tissue sections, GFAP **(b)** and Iba1 **(c)** images show a moderate and confined immune reaction in both AAV2-hAADC-treated (left) and control (middle) NHP. However, some cellular infiltration is evident in the animal with infusate leakage into the internal capsule (right, **a–c**). Black squares indicate **(a′)** H&E, **(b′)** GFAP, and **(c′)** Iba1 staining at higher magnification for both AAV2-hAADC and PBS control animals. *Inset* on the right in **(a′)** demonstrates the presence of some eosinophils in the infusate leakage area (black square). Arrows in **(a–c)** (left images) show slight cellular infiltration exclusively around a blood vessel near the putaminal cannula tract. GFAP-immunostained sections **(b** and **b′)** were counterstained with cresyl violet. Scale bars: **(a–c)** 2 mm; **(a′–c′)** 100 μm; *inset*, 20 μm. Color images available online at www.liebertonline.com/hum

The vector dose for the animals in the present study was 7.0×10^{11} VG (infused unilaterally), a 2-fold higher total vector dose than that received by high-dose phase I trial patients (Table 1). No animals infused with AAV2-hAADC in the present study developed any adverse effects or signs of toxicity related to the vector. All the animals remained healthy (i.e., no weight loss) throughout the study and exhibited only the behavioral signs expected in mildly hemi-MPTP-lesioned parkinsonian animals. In fact, if anything, their parkinsonism tended to ameliorate after AAV2-hAADC infusion (mean CRS before surgery, 10 ± 3; mean CRS ~8 months after surgery, 8 ± 4). All the animals were responsive to L-DOPA before and after the surgery and, although they received many L-DOPA doses, none of the animals exhibited L-DOPA-induced dyskinesia (see supplementary material; supplementary data are available online at www.liebertonline.com/hum).

The postmortem analysis of the tissue revealed a broad distribution of AADC expression in the putamen and caudate nucleus that closely overlapped areas of Gd signal observed during infusion, with a large number of AADC-positive striatal neurons and fibers evident (Fig. 2a). Infusate was well contained within both target structures in all animals, even though the relative infusion volume was larger

Table 1. Vector Doses Administered in Preclinical and Clinical Studies

Study	*Dose*	*Target*	*Sites/hemis.*	V_i*/hemis. (μl)*	*VG/hemis.*	*Total VG* ($\times 10^9$)
Present study		pr.c. Cd/Put	2 (UL)	100	7.0×10^{11}	700
NHP safety (Forsayeth *et al.*, 2006)	Lowest	c./pt.c. Put	2 (BL)	100	6.0×10^{9}	12
	Highest	c./pt.c. Put	2 (BL)	100	5.0×10^{11}	1000
Clinical phase 1 (Christine *et al.*, 2009)	Low	pt.c. Put	2 (BL)	100	4.5×10^{10}	90
	High	pt.c. Put	2 (BL)	100	1.5×10^{11}	300

BL, bilateral; c., commissural; Cd, caudate nucleus; hemis., hemisphere; NHP, nonhuman primate; pr.c., precommissural; pt.c., postcommissural; Put, putamen; UL, unilateral; VG, vector genomes; V_i, infusion volume.

for the caudate nucleus, a small structure compared with the putamen. As mentioned previously, one of the animals that received AAV2-hAADC exhibited significant leakage into the internal capsule and histological signs of infection in the same area. Nevertheless, a large number of medium spiny neurons and fibers were found in both caudate nucleus and putamen (Fig. 2b). We noted some AADC expression in neuronal cell bodies and fibers in structures within the infused hemisphere, such as in the internal and external globus pallidus, subthalamic nucleus, and substantia nigra pars reticulata (data not shown), indicating anterograde transport of the vector (Ciesielska *et al.*, 2011).

Discussion

The purpose of this study was to determine the long-term safety of a new, image-guided parenchymal acute delivery system for AAV vectors. Previous clinical experience has indicated that inadequate distribution of transgene expression in the putamen may be responsible for discrepancies in efficacy between NHP and human subjects (Christine *et al.*, 2009; Bartus *et al.*, 2011). Accordingly, we have sought to improve vector distribution by means of visual surrogate markers that permit intraoperative monitoring of infusions (Richardson *et al.*, 2009). This innovation enabled quantitative analyses of dynamic parameters that influence parenchymal vector distribution, such as ventricular leakage and cannula reflux (Varenika *et al.*, 2009), as well as optimal cannula placement (Yin *et al.*, 2010, 2011) and rate of infusion (Varenika *et al.*, 2009). These investigations led to the development of a clinical platform for MRI-monitored CED in the brain. This system integrates three component technologies: the SmartFlow catheter, a custom-designed, ceramic, fused silica cannula with a 3-mm stepped tip that makes it reflux-resistant; the SmartFrame, which is an MRI-guided adjustable trajectory frame; and ClearPoint software, a software system that detects gadolinium fiducials housed in the SmartFrame and communicates the frame position to the MRI console, thereby allowing the operator to align the frame to the target trajectory (see Richardson *et al.*, 2011a, for details). The combination of these three components results in improved control of infusate delivery and visualization of therapeutic distribution.

The purpose of the present study was to test the safety of the entire system in the context of delivering AAV2-hAADC into the parkinsonian monkey putamen. It was unnecessary to conduct an efficacy study of AAV2-hAADC in NHP because that has been abundantly established (Bankiewicz *et al.*, 2006; Forsayeth *et al.*, 2006; Hadaczek *et al.*, 2010). These data form the basis of a proposed clinical trial of AAV2-hAADC in PD with the recognition that the delivery technique in previous phase I studies (Eberling *et al.*, 2008; Christine *et al.*, 2009; Muramatsu *et al.*, 2010) was unable to ensure sufficient distribution and transgene expression to be able to achieve optimal non-rate-limiting AADC activity in transduced tissue (Forsayeth *et al.*, 2006). The experiments in this paper show the safety and tolerability of administering a higher dose of AAV2-hAADC under real-time MR imaging guidance CED in the precommissural striatum of parkinsonian NHP with an optimized clinical cannula. There were no behavioral or histological indications of parenchymal injury due to cannula insertion, despite two cannula insertions occurring close to each other in the same hemisphere of every animal. Only in one case, out of 10, did we detect significant leakage of the infusate into the internal capsule, where some cellular infiltration was revealed by H&E staining, suggesting an infection, although it was asymptomatic. In our experience, the NHP putamen and other smaller nuclei are inappropriate targets for testing the larger infusion volumes proposed for clinical study ($>200\,\mu$l per site), due to leakage beyond the anatomic boundaries of these small targets. Of the two infusion sites in this study, the caudate nucleus was the smaller, receiving $50\,\mu$l of infusate, and this was well tolerated. Even though the caudate nucleus will not be targeted in clinical trials, the fact that the infusion in this small structure was uneventful and well tolerated further demonstrates the safety of the delivery system tested in the present work. However, the V_d/V_i ratio obtained from MRI images for this region was lower than expected (V_d/V_i caudate nucleus, 1.6). Leakage into the lateral ventricle during the caudate infusion seemed to be absent because we could see a well-contained Gd signal in the MR images. However, as previously described by Song and Lonser (2008), infusate leakage into the ventricle is not detected on T_1-weighted MRI but only on fluid-attenuated inversion MRI. Because we did not acquire this kind of sequence, we cannot rule out the possibility that some undetected infusate extravasation into the lateral ventricle occurred, and this may explain the low V_d/V_i determined for the caudate nucleus. Even so, we observed robust AADC expression in all test animals. Our data support the value of real-time image-guided drug delivery to ensure the most accurate and predictable delivery of therapeutic drugs directly into the brain parenchyma. To optimize distribution of AAV2 vectors via CED within the human putamen, we propose delivery of $900\,\mu$l across four infusion sites (two sites per hemisphere). This increase in vector volume is consistent with the difference in the volume of the putamen between humans and NHP. Overall, these data provide

additional support for a clinical study with the highest vector dose previously approved for clinical study. A clinical dose of 9.0×10^{11} VG has an extrapolated safety margin of more than 5-fold relative to the current study.

Intracranial hemorrhage is a common risk of stereotactic craniotomy (Binder *et al.*, 2005) and was also seen in the AAV2-hAADC phase I clinical trial patients with PD (Christine *et al.*, 2009; Muramatsu *et al.*, 2010). Similarly, one of our PBS control animals presented with a possible hemorrhage in the putamen detected only postmortem. The fact that the putamen is profusely irrigated by lenticulostriate arteries, which branch from the middle cerebral artery, makes the putaminal region prone to hemorrhagic strokes (Feekes and Cassell, 2006). Because the iMRI ClearPoint system also allows the clinical team to identify large blood vessels and make any necessary adjustments to the cannula trajectories, the potential for hemorrhages should be reduced. The present technique also provides rapid feedback on the physical and anatomic diffusion parameters important for optimizing gene transfer (Richardson *et al.*, 2011b).

All animals receiving AAV2-hAADC infusion showed good coverage of the target structures, both caudate nucleus and putamen, whereas the striatum of control animals was devoid of AADC signal on the lesioned side after the PBS infusion. In contrast to previous studies in our laboratory (Richardson *et al.*, 2011a,b), striatal AADC expression did not perfectly match gadolinium signal on MRI. The region of AADC immunostaining in the striatum was somewhat greater than indicated by MR images. This phenomenon could be due to a discrepancy between the postsurgical interval in previous and present studies; that is, 1–5 weeks previously and $\sim$8 months in the present study. We have previously reported that the AAV2-hAADC distribution appears to broaden slowly over time in NHP, resulting in a larger coverage of target regions (Daadi *et al.*, 2006). In addition, because AAV2 vector is transported anterogradely through the axons (Ciesielska *et al.*, 2011), we also found AADC expression in structures outside the striatum such as the globus pallidus, subthalamic nucleus, substantia nigra pars reticulata, and thalamus.

We also tested a relative vector dose higher than the highest dose administered to patients in the phase I trial (Christine *et al.*, 2009). Animals slightly improved their parkinsonism after receiving AAV2-hAADC, because study animals were only mildly lesioned with MPTP in contrast to preclinical efficacy studies in which animals were severely overlesioned (Bankiewicz *et al.*, 2006; Forsayeth *et al.*, 2006). This high vector dose (7.0×10^{11} VG) resulted in strong AADC expression in the striatum. The possible toxic effect of such a high AAV vector dose was ruled out because we did not find any signs of tissue damage related to the high vector dose in any of the treated animals. Also, all animals remained free of L-DOPA-induced dyskinesia or other adverse effects. Both GFAP and Iba1 immunostaining and H&E staining were consistent with insertion of the cannula into the target structures, with no pathological changes that could be attributed to AAV2-hAADC. We also did not observe any behavioral adverse effects, even though we dosed animals for long periods of time (1-month regimens on two occasions after treatment) with oral L-DOPA. This study confirms the safety of the combination of the SmartFlow cannula positioned via the ClearPoint system with a high AAV2-hAADC dose directing broad expression of AADC throughout the NHP putamen. These data are supportive of clinical evaluation of this advanced vector delivery system in a planned phase II study in PD.

Acknowledgments

The authors thank Peter Piferi and Geoffrey Bates of MRI Interventions (formerly Surgivision) for providing the ClearPoint equipment and for assistance in this study. This work was supported by NIH grant R01NS050156 to K.S.B.

Author Disclosure Statement

Authors have no conflicts of interest.

References

Bankiewicz, K.S., Oldfield, E.H., Chiueh, C.C., *et al.* (1986). Hemiparkinsonism in monkeys after unilateral internal carotid artery infusion of 1-methyl-4-phenyl-1,2,3,6-tetrahydropyridine (MPTP). Life Sci. 39, 7–16.

Bankiewicz, K.S., Eberling, J.L., Kohutnicka, M., *et al.* (2000). Convection-enhanced delivery of AAV vector in parkinsonian monkeys: *In vivo* detection of gene expression and restoration of dopaminergic function using pro-drug approach. Exp. Neurol. 164, 2–14.

Bankiewicz, K.S., Forsayeth, J., Eberling, J.L., *et al.* (2006). Long-term clinical improvement in MPTP-lesioned primates after gene therapy with AAV-hAADC. Mol. Ther. 14, 564–570.

Bartus, R.T., Herzog, C.D., Chu, Y., *et al.* (2011). Bioactivity of AAV2-neurturin gene therapy (CERE-120): Differences between Parkinson's disease and nonhuman primate brains. Mov Disord 26, 27–36.

Binder, D.K., Rau, G.M., and Starr, P.A. (2005). Risk factors for hemorrhage during microelectrode-guided deep brain stimulator implantation for movement disorders. Neurosurgery 56, 722–732; discussion 722–732.

Bobo, R.H., Laske, D.W., Akbasak, A., *et al.* (1994). Convection-enhanced delivery of macromolecules in the brain. Proc. Natl. Acad. Sci. U.S.A. 91, 2076–2080.

Christine, C.W., Starr, P.A., Larson, P.S., *et al.* (2009). Safety and tolerability of putaminal AADC gene therapy for Parkinson disease. Neurology 73, 1662–1669.

Ciesielska, A., Mittermeyer, G., Hadaczek, P., *et al.* (2011). Anterograde axonal transport of AAV2-GDNF in rat basal ganglia. Mol. Ther. 19, 922–927.

Daadi, M.M., Pivirotto, P., Bringas, J., *et al.* (2006). Distribution of AAV2-hAADC-transduced cells after 3 years in Parkinsonian monkeys. Neuroreport 17, 201–204.

Eberling, J.L., Jagust, W.J., Taylor, S., *et al.* (1998). A novel MPTP primate model of Parkinson's disease: Neurochemical and clinical changes. Brain Res. 805, 259–262.

Eberling, J.L., Jagust, W.J., Christine, C.W., *et al.* (2008). Results from a phase I safety trial of hAADC gene therapy for Parkinson disease. Neurology 70, 1980–1983.

Feekes, J.A., and Cassell, M.D. (2006). The vascular supply of the functional compartments of the human striatum. Brain 129, 2189–2201.

Fiandaca, M., Forsayeth, J., Dickinson, P., and Bankiewicz, K. (2008). Image-guided convection-enhanced delivery platform in the treatment of neurological diseases. Neurotherapeutics 5, 123–127.

Fiandaca, M., Varenika, V., Eberling, J., *et al.* (2009). Real-time MR imaging of adeno-associated viral vector delivery to the primate brain. Neuroimage 47, T27–T35.

Forsayeth, J.R., Eberling, J.L., Sanftner, L.M., *et al.* (2006). A dose-ranging study of AAV-hAADC therapy in parkinsonian monkeys. Mol. Ther. 14, 571–577.

Gimenez, F., Krauze, M.T., Valles, F., *et al.* (2011). Image-guided convection-enhanced delivery of GDNF protein into monkey putamen. Neuroimage 54(Suppl. 1), S189–S195.

Hadaczek, P., Eberling, J.L., Pivirotto, P., *et al.* (2010). Eight years of clinical improvement in MPTP-lesioned primates after gene therapy with AAV2-hAADC. Mol. Ther. 18, 1458–1461.

Imbert, C., Bezard, E., Guitraud, S., *et al.* (2000). Comparison of eight clinical rating scales used for the assessment of MPTP-induced parkinsonism in the macaque monkey. J. Neurosci. Methods 96, 71–76.

Krauze, M.T., Saito, R., Noble, C., *et al.* (2005). Reflux-free cannula for convection-enhanced high-speed delivery of therapeutic agents. J. Neurosurg. 103, 923–929.

Matsushita, T., Elliger, S., Elliiger, C., *et al.* (1998). Adeno-associated virus vectors can be efficiently produced without helper virus. Gene Ther. 5, 938–945.

Muramatsu, S., Fujimoto, K., Kato, S., *et al.* (2010). A phase I study of aromatic L-amino acid decarboxylase gene therapy for Parkinson's disease. Mol. Ther. 18, 1731–1735.

Richardson, R.M., Varenika, V., Forsayeth, J.R., and Bankiewicz, K.S. (2009). Future applications: Gene therapy. In *Intraoperative MRI in Functional Neurosurgery*. P.S. Larson and D.A. Lim, eds. (W. B. Saunders, Philadelphia, PA) *pp*. 219–224.

Richardson, R.M., Kells, A.P., Martin, A.J., *et al.* (2011a). Novel platform for MRI-guided convection-enhanced delivery of therapeutics: Preclinical validation in nonhuman primate brain. Stereotact. Funct. Neurosurg. 89, 141–151.

Richardson, R.M., Kells, A.P., Rosenbluth, K.H., *et al.* (2011b). Interventional MRI-guided putaminal delivery of AAV2-GDNF for a planned clinical trial in Parkinson's disease. Mol. Ther. 19, 1048–1057.

Sanchez-Pernaute, R., Harvey-White, J., Cunningham, J., and Bankiewicz, K.S. (2001). Functional effect of adeno-associated virus mediated gene transfer of aromatic L-amino acid decarboxylase into the striatum of 6-OHDA-lesioned rats. Mol. Ther. 4, 324–330.

Song, D.K., and Lonser, R.R. (2008) Convection-enhanced delivery for treatment of pediatric neurologic disorders. J. Child. Neurol. 23, 1231–1237.

Su, X., Kells, A.P., Huang, E.J., *et al.* (2009). Safety evaluation of AAV2-GDNF gene transfer into the dopaminergic nigrostriatal pathway in aged and parkinsonian rhesus monkeys. Hum. Gene Ther. 20, 1627–1640.

Valles, F., Fiandaca, M.S., Eberling, J.L., *et al.* (2010). Qualitative imaging of adeno-associated virus serotype 2-human aromatic L-amino acid decarboxylase gene therapy in a phase I study for the treatment of Parkinson disease. Neurosurgery 67, 1377–1385.

Varenika, V., Kells, A.P., Valles, F., *et al.* (2009). Controlled dissemination of AAV vectors in the primate brain. Prog. Brain Res. 175, 163–172.

Wright, J., Qu, G., Tang, C., and Sommer, J. (2003). Recombinant adeno-associated virus: Formulation challenges and strategies for a gene therapy vector. Curr. Opin. Drug Discov. Dev. 6, 174–178.

Yin, D., Valles, F.E., Fiandaca, M.S., *et al.* (2009). Striatal volume differences between non-human and human primates. J. Neurosci. Methods 176, 200–205.

Yin, D., Richardson, R.M., Fiandaca, M.S., *et al.* (2010). Cannula placement for effective convection-enhanced delivery in the non-human primate thalamus and brainstem: Implications for clinical delivery of therapeutics. J. Neurosurg. 113, 240–248.

Yin, D., Valles, F.E., Fiandaca, M.S., *et al.* (2011). Optimal region of the putamen for image-guided convection-enhanced delivery of therapeutics in human and non-human primates. Neuroimage 54(Suppl. 1), S196–S203.

Address correspondence to:
Dr. Krystof S. Bankiewicz
Department of Neurological Surgery
University of California San Francisco
1855 Folsom Street, MCB 226
San Francisco, CA 94103-0555

E-mail: Krystof.Bankiewicz@ucsf.edu

Received for publication August 30, 2011;
accepted after revision October 15, 2011.

Published online: October 21, 2011.